Electronic Supplementary Material (ESI) for Environmental Science: Nano.

Nanoscale Observations of Fe(II)-Induced Ferrihydrite Transformation

Odeta Qafoku*[a], Libor Kovarik[b], Mark E. Bowden[a], Elias Nakouzi[b], Anxu Sheng[c], Juan Liu[c], Carolyn I. Pearce[b], Kevin M. Rosso[b]

[a]Environmental Molecular Sciences Laboratory, Pacific Northwest National Laboratory, Richland, WA 99352, USA
[b]Pacific Northwest National Laboratory, Richland, WA 99352, USA
[c]College of Environmental Sciences and Engineering, Peking University, Beijing 100871, China

Submitted to Environmental Science: Nano

The Geochemist's Workbench® MINTEQ thermodynamic database

MINTEQ dataset is the thermodynamic database from Visual MINTEQ release 2.40, for use with the GWB programs, compiled in December 2005 and maintained by Jon Petter Gustafsson, KTH (Royal Institute of Technology), Stockholm, Sweden.

Log K values are calculated as functions of temperature using the van't Hoff equation and reflect dissociation/dissolution reactions. Mineral saturation indices are reported as log Q/K, Q and K are respectively reaction's activity product and equilibrium constant.

To accurately represent conditions of experiments in this study, we performed geochemical calculations maintaining fixed HCO_3 concentrations while allowing pCO_2 concentration to float. Calculations were performed at ambient temperature; solids saturated during the calculations were not allowed to precipitate.

X-Ray Diffraction Methods

Diffraction patterns were collected from capillary specimens using a Rigaku D-Max II Rapid microbeam diffractometer with a rotating Cr anode source (λ=2.2910 Å). Estimates of phase fractions and crystallite size were obtained using Rietveld (whole pattern) fitting with the program TOPAS (Bruker AXS). Patterns for lepidocrocite and goethite were calculated using structures from the International Crystal Structure Database (ICSD, Fachinformationszentrum Karlsruhe, Germany). The structure for lepidocrocite was in space group *Cmcm* reported by Christensen *et al*. (1982). The structure for Goethite was in *Pbnm* reported by Yang *et al*. (2006).

Ferrihydrite was not explicitly modelled but its broad diffraction features were fitted with 2 unquantified pseudo-Voigt peaks. Some contribution was undoubtedly also included in the background. The ferrihydrite concentration was determined by difference, based on the intensities of lepidocrocite and goethite. When the combined refined scale factors of these two components were at a maximum, their concentrations were defined to be a total of 100%. This gave a basis for determining their concentrations at other times, and ferrihydrite was assumed to be the difference. The baseline (including some of the ferrihydrite) was fitted with a 15 order Chebyshev polynomial. The relatively large number of parameters was required to account for the complex background, which included contributions from the capillary, water, and ferrihydrite. An example of a background fit (before appreciable goethite or lepidocrocite forms) is show in figure S4 (A).

The approach was not intended to be a perfect Rietveld quantification, but will provide reliable trends given the experimental constraints and the uncertainty of the ferrihydrite structure.

Variations in the diffraction peak breadths indicated that the crystallites of lepidocrocite and goethite had an anisotropic shape, as might be expected from their crystallography and common habit. To model this, and obtain estimates of crystallite size, anisotropic broadening was applied using the TOPAS macros published by Ectors et al. (2015). This is a variance slope apparent size based on dividing crystallite volume by projected area. The values reported are the mean principle orthogonal axis lengths (the radii r_x, r_y, and r_z in Ectors' formulation), which in our fit were aligned to the crystallographic axes *a*, *b*, and *c* respectively. The broadening was applied to peak shapes calculated using the TOPAS fundamental parameters approach and calibrated for instrumental shape using a pattern collected from a capillary specimen of LaB_6 (NIST SRM 660A).

Crystallites with radii as small as 1nm could be measured using this technique. Figures S4 (B) and S4 (C) show fits of nascent goethite where constraining the crystallites to a 2nm results in a noticeably poorer fit. Further Rietveld fits are shown in figures S4 (D) and (E) for longer times when greater quantities of crystalline compounds are apparent. Although there is some minor residual misfit, these examples demonstrate the quality of the fitting which is certainly suitable for our purpose of showing trends in the development of crystalline compounds during aging of ferrihydrite.

Suspension conditions	Experiment 1			Experiment 2		
	Fe(II)-source 0.5mM	$NaHCO_3$ mM (sample ID)		Fe(II)-source 0.5mM	$NaHCO_3$ mM	
Fh density 1g/L 10mM PIPES buffer pH 7	Chloride	no-bicarbonate ($Cl_{NO}HCO_3$)	0	Sulfate	no-bicarbonate ($SO_{4NO}HCO_3$)	0
		low-bicarbonate ($Cl_{LOW}HCO_3$)	0.168		low-bicarbonate ($SO_{4LOW}HCO_3$)	0.168
		mid-bicarbonate ($Cl_{MID}HCO_3$)	1		mid-bicarbonate ($SO_{4MID}HCO_3$)	1
		high-bicarbonate ($Cl_{HIGH}HCO_3$)	10		high-bicarbonate ($SO_{4HIGH}HCO_3$)	10

Table S1 The experimental design to study Fh transformation mediated by Fe(II). Solution was analyzed for Fe(II); solids were analyzed with BET, XRD, SEM, and TEM for formation of new crystalline products.

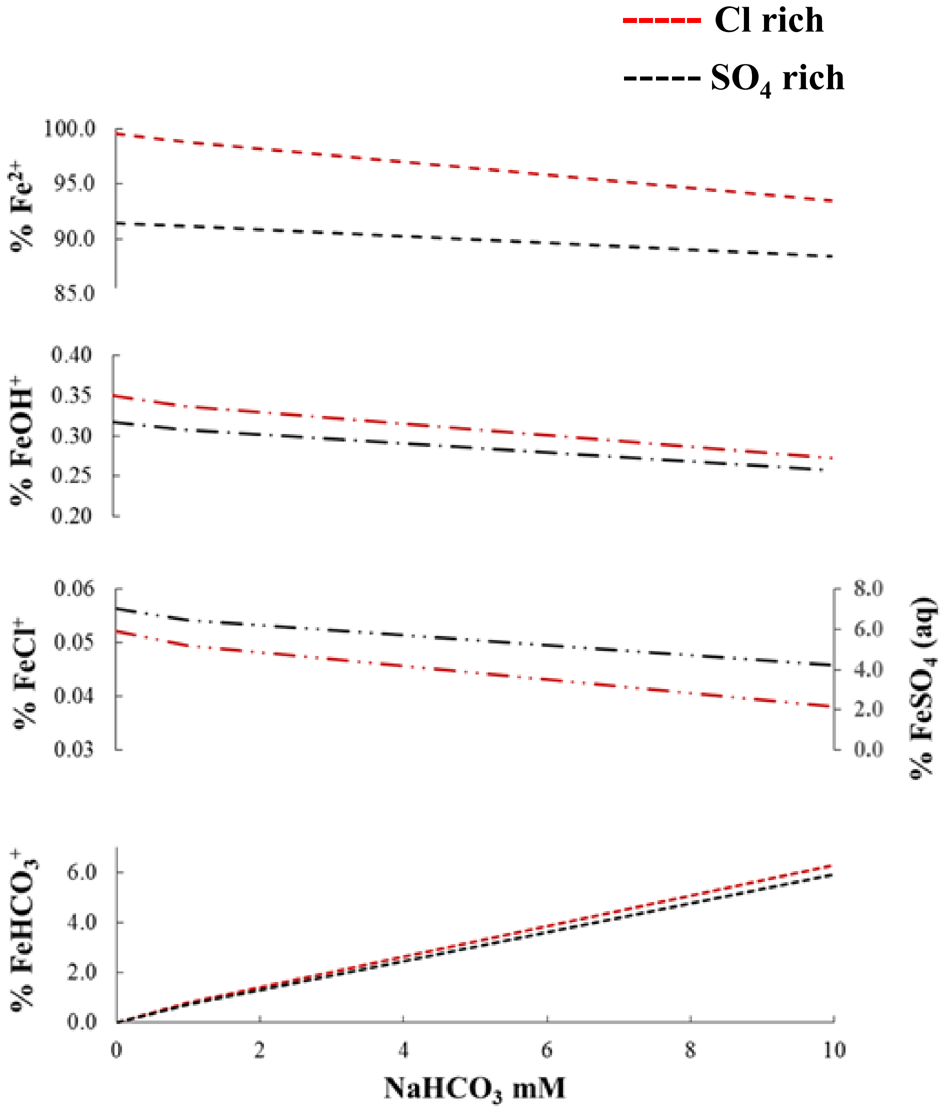

Fig. S1 Aqueous speciation of 0.5mM $FeCl_2$ and 0.5mM $FeSO_4$ with increasing $NaHCO_3$ concentration. Formation of $FeSO_4$(aq) was at the expense of reactive Fe(II) and decreased with increasing $FeHCO_3^+$ in solution.

Sample ID	Treatment		--------------------------------Surface Area m^2/g--------------------------------------								
	Fe-source	$NaHCO_3$ mM	0.3h	1h	2h	3h	4h	8h	2d	5d	15d
$_{NO}HCO_3$	$FeCl_2$	0	220.04	270.95	228.29	236.27	223.05	78.15	25.32	8.60	28.34
$_{HIGH}HCO_3$		10	157.95	277.69	256.29	121.37	164.10	122.37	46.53	41.60	31.73
$_{NO}HCO_3$	$FeSO_4$	0	329.64	294.19	282.53	258.90	240.76	79.62	76.20	75.29	27.23
$_{HIGH}HCO_3$		10	292.84	295.84	259.02	257.31	188.14	175.45	47.83	25.74	27.33

Table S2 Evolution of surface area with time, during reaction of 2-line Fh with $FeCl_2$ or $FeSO_4$, with or without HCO_3 as a co-anion

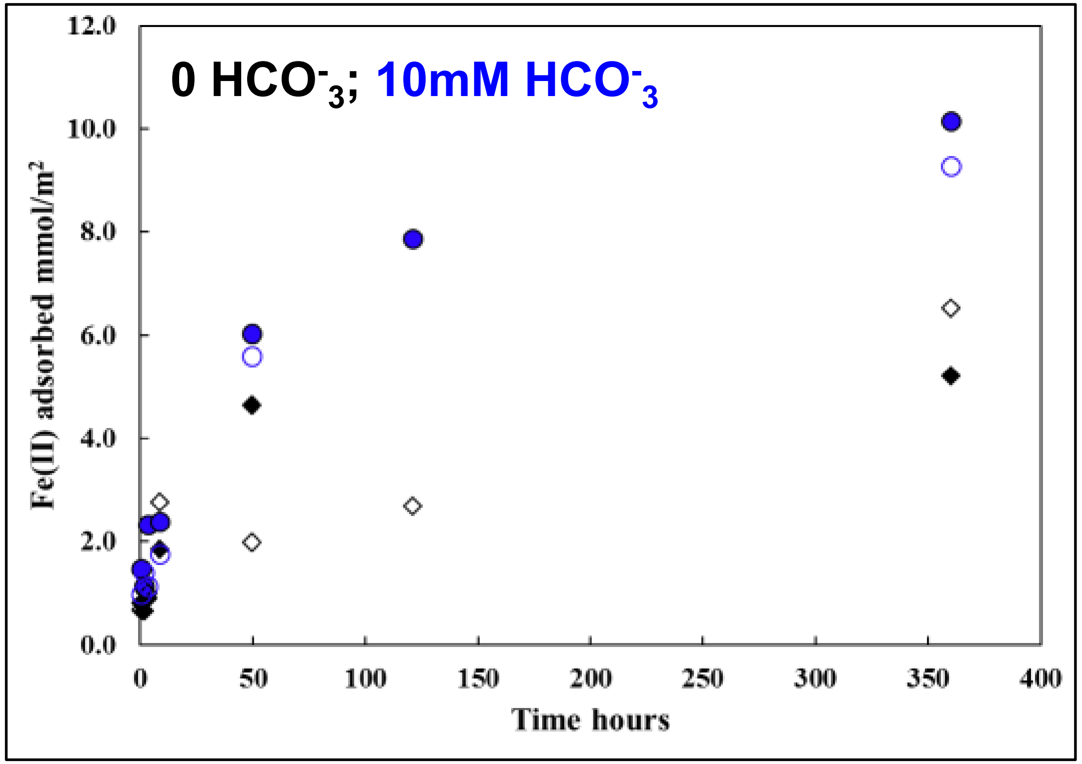

Fig. S2 Fe(II) adsorption by 2-line Fh, normalized by surface area of reaction products. Suspension density of 1g/L and pH 7 (adjusted by PIPES buffer). Filled symbols show results in 0.5 mM $FeCl_2$ and open symbols in $FeSO_4$.

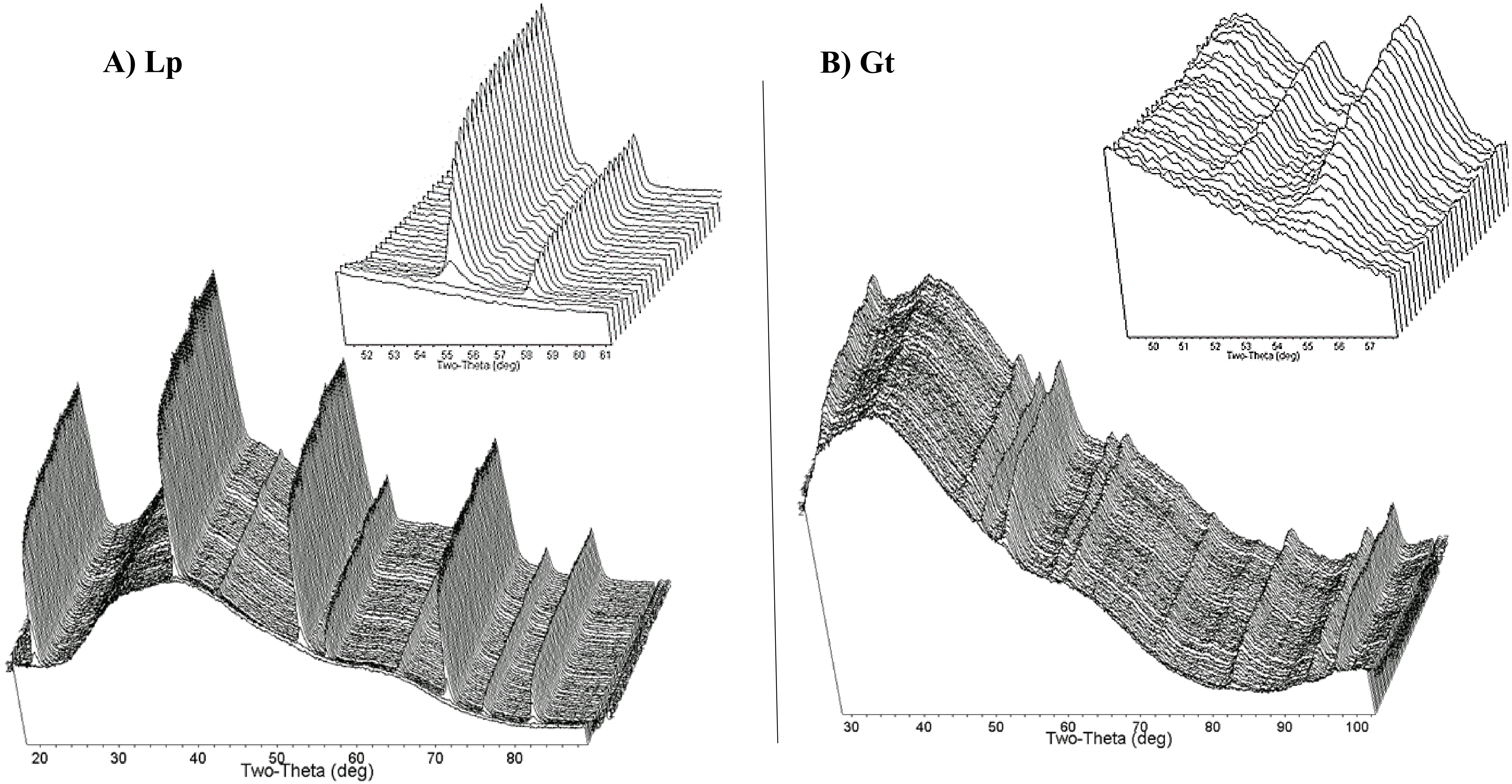

Fig. S3. 3D µXRD patterns show A-Lp evolution, for $Cl_{NO}HCO_3$ experiment; and B-Gt evolution for $Cl_{HIGH}HCO_3$ experiment, from 0 to 62 h (inserts from 0 to 25 hours).

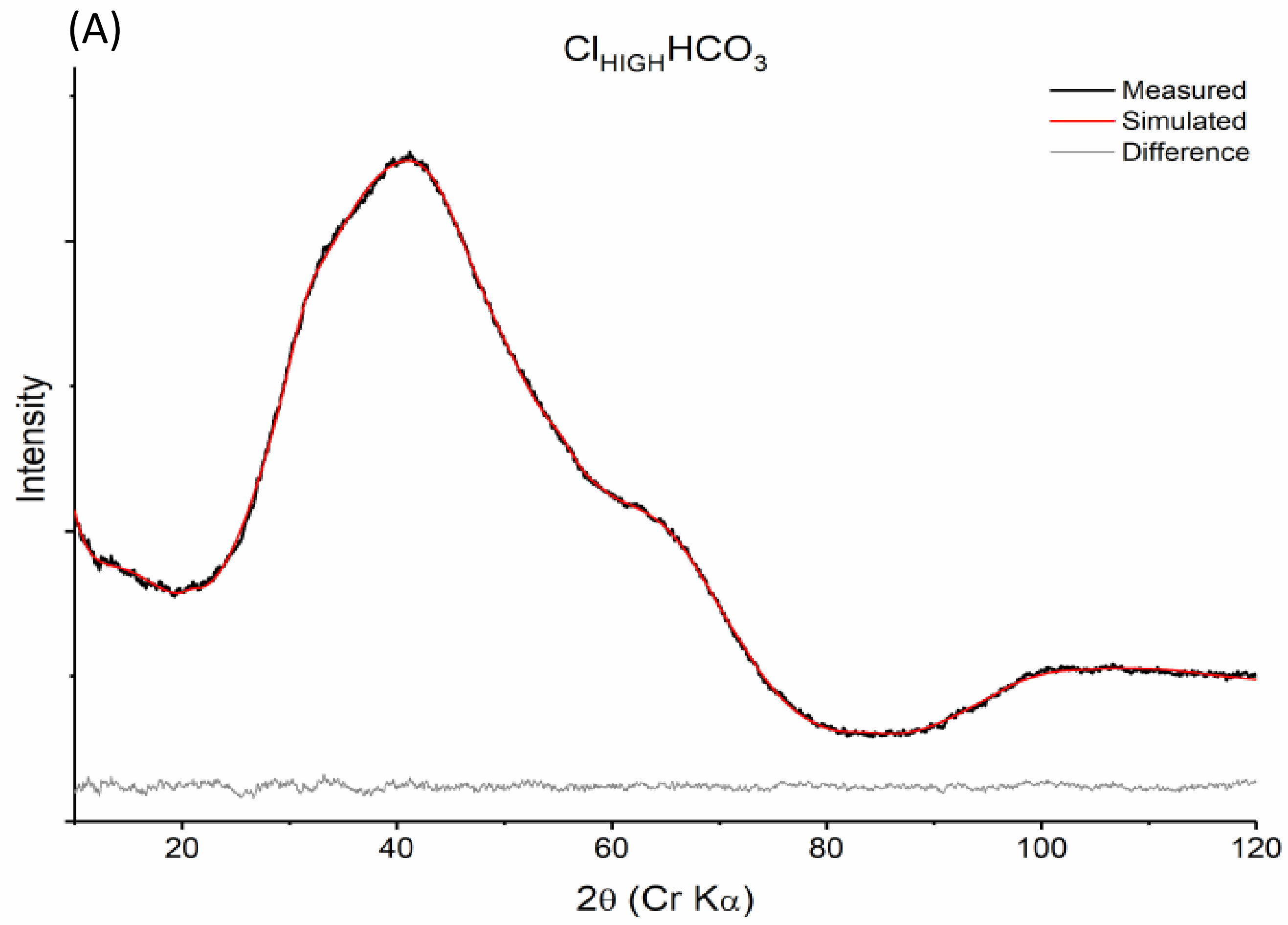

Fig. S4 (**A**). XRD fit of $Cl_{HIGH}HCO_3$ before detection of crystalline compounds, demonstrating the background fit. R_{wp} = 0.608%.

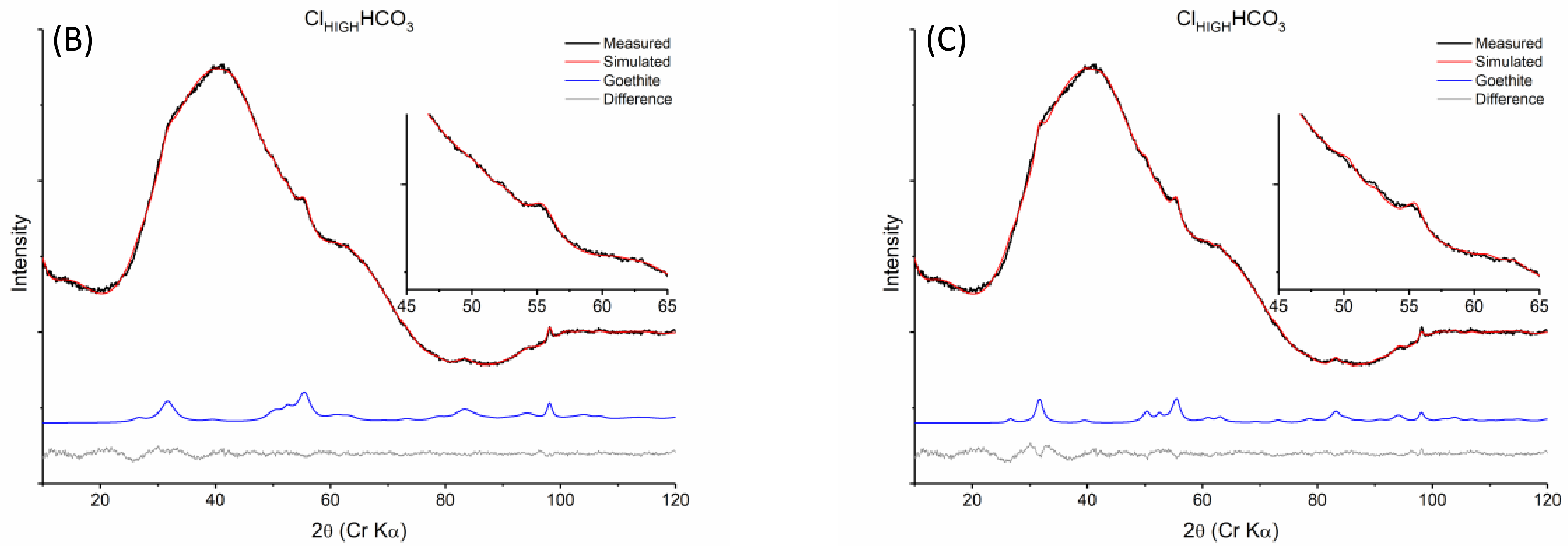

Fig. S4. (**B**) XRD fit of $Cl_{HIGH}HCO_3$ at 3h with fit of goethite ($r_x \times r_y \times r_z = 1 \times 1 \times 3.5$ nm). The inset shows detail of a region where the (130), (021), (040), and (111) peaks dominate and their breadth is strongly influenced by the r_x and r_y dimensions. $R_{wp} = 0.513$ %. (**C**) XRD fit of $Cl_{HIGH}HCO_3$ at 3h with goethite constrained to have crystallite dimensions 2 × 2 × 3.5 nm. The inset shows the fit is considerably poorer than in (B) with $R_{wp} = 0.591$ %.

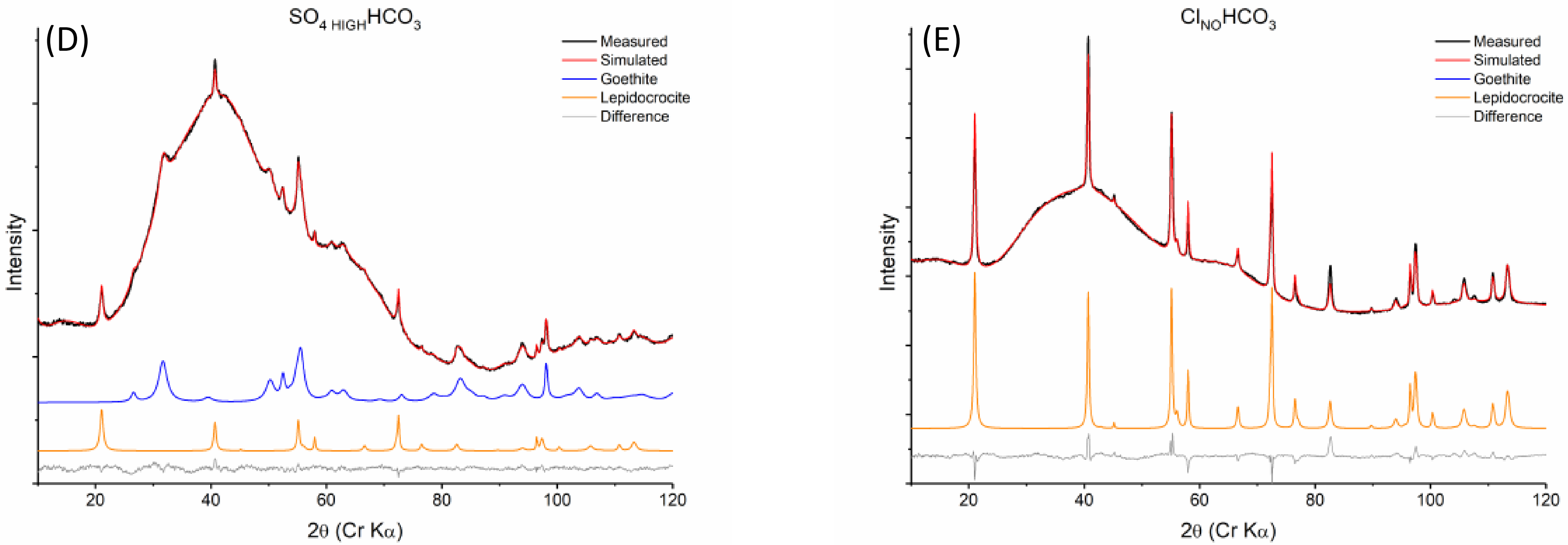

Fig. S4. (**D**) XRD fit of SO$_{4\ \mathrm{HIGH}}$HCO$_3$ at 48h, demonstrating a larger quantity of goethite mixed with lepidocrocite (17%). Rwp = 0.532 %. (**E**) XRD fit of Cl$_{\mathrm{NO}}$HCO$_3$ at 48h showing a substantial quantity of large (20 × 6.6 × 18 nm) lepidocrocite crystallites. Rwp = 1.564 %.

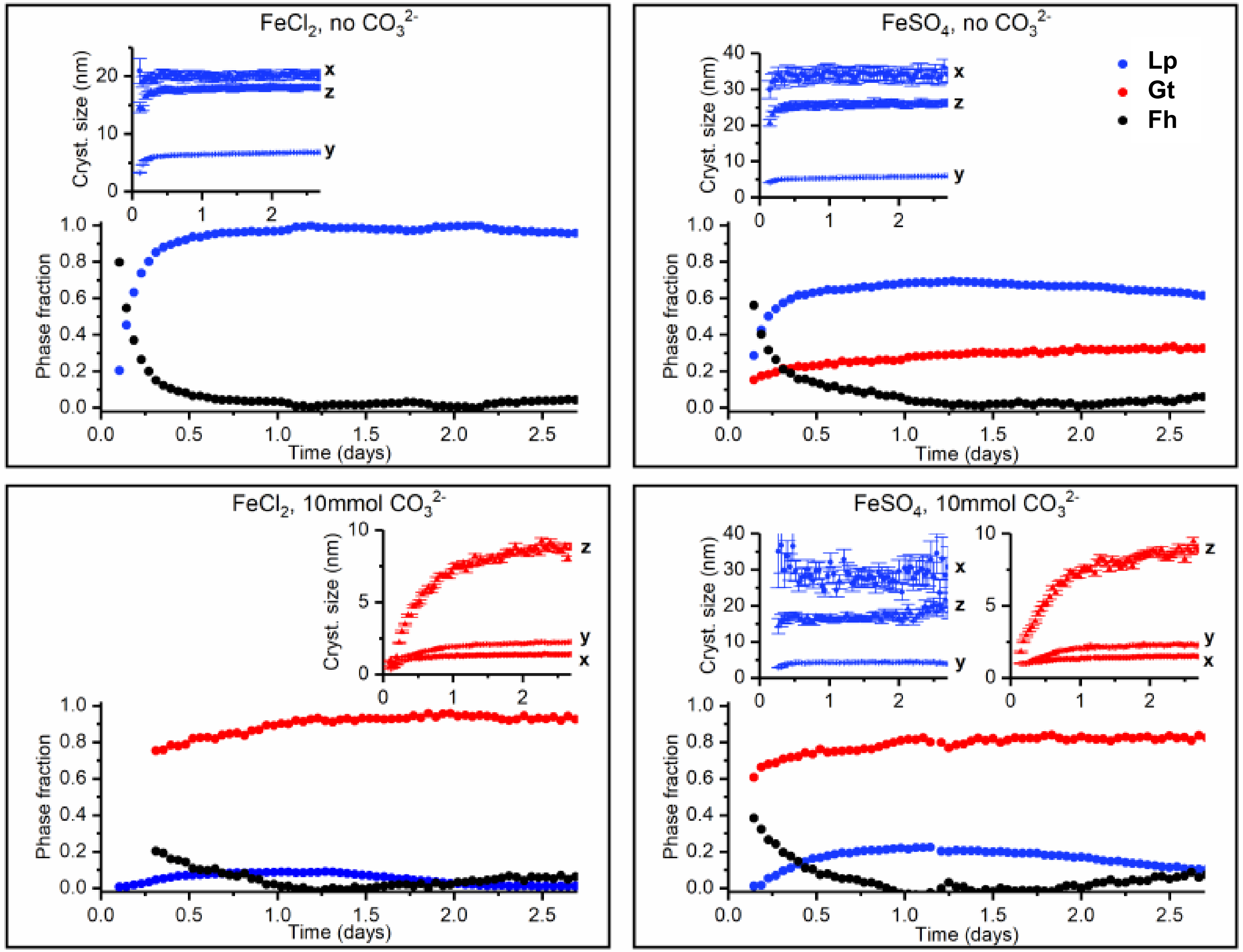

Fig. S5 Real time *in situ* µ-XRD showing evolution of and transformation of Fh mediated by Fe(II) at 2.5d reaction. The crystallite dimensions, x-length, y-thickness, z-across, for Lp and Gt are also shown.

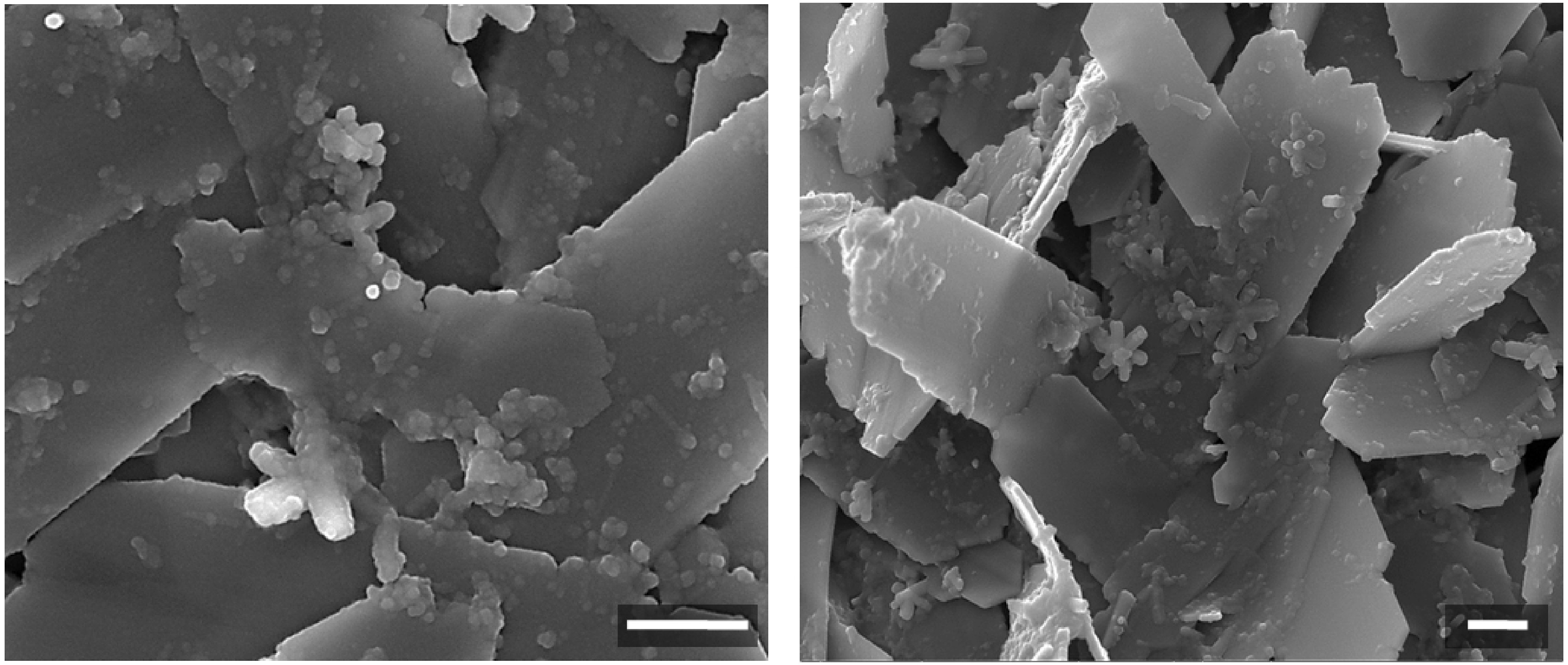

Fig. S6 SEM images at 8.5 h, show Lp is the major product formed during Fh transformation catalyzed by 0.5 mM Fe(II) with Cl^- as a counteranion. However, at this reaction time distinct rod-like crystals appear, consistent with the typical morphology of Gt. Scale bar =200 nm.

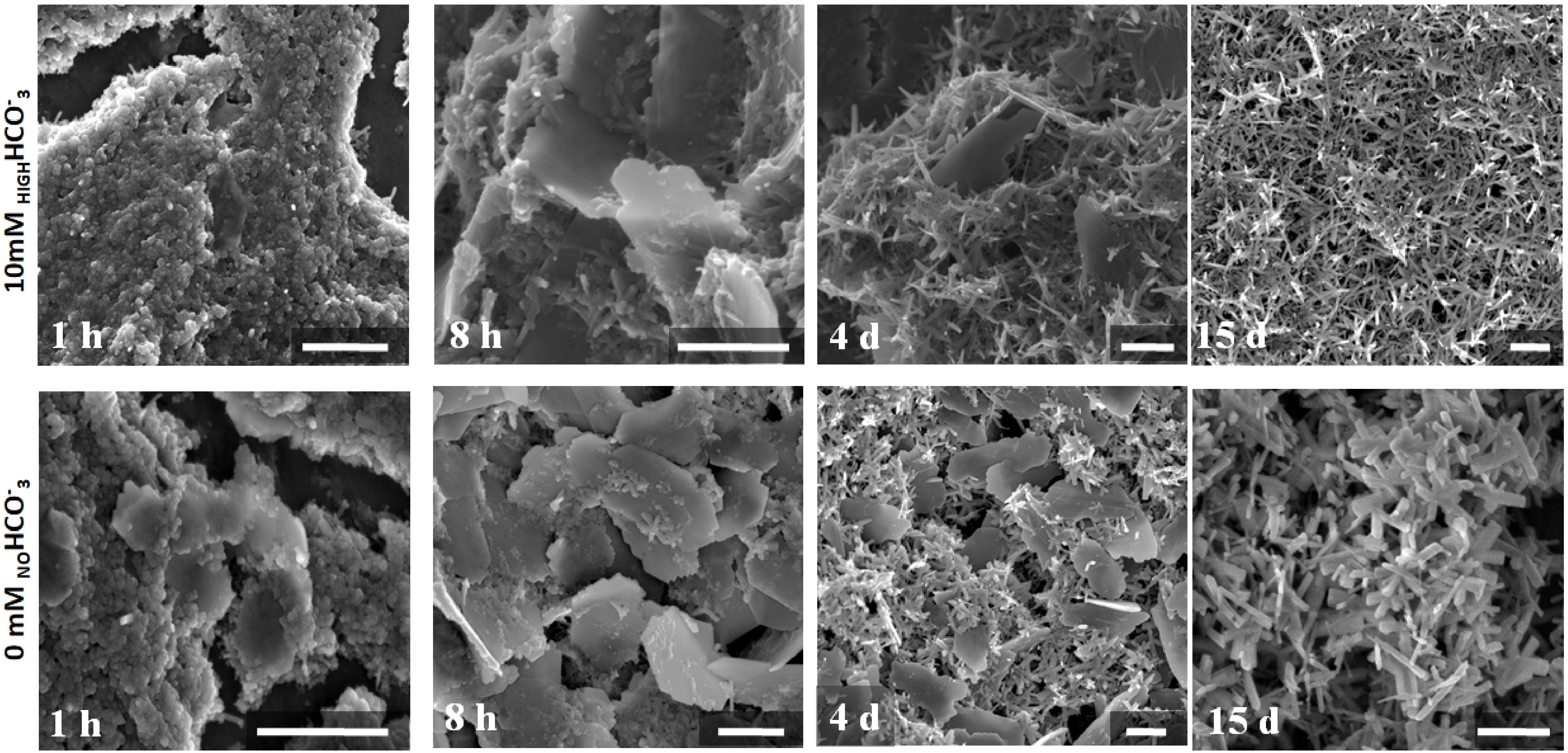

Fig. S7 Sequential SEM images reveal Fh transformation catalyzed by 0.5 mM Fe(II) with SO_4^{2-} as a counteranion (bottom row). Addition of bicarbonate and its effect in the evolution of Lp and Gt is shown on top row. Scale bar =500nm.

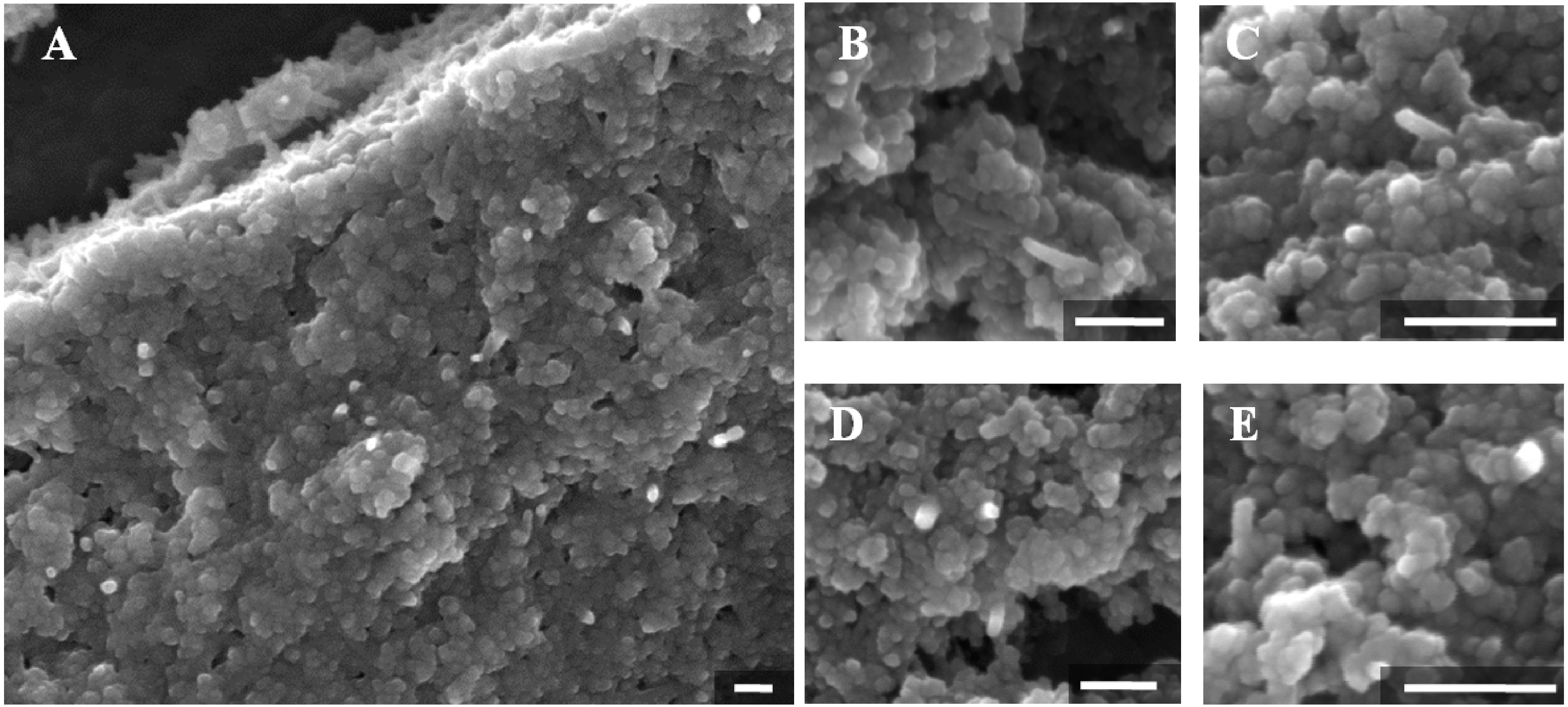

Fig. S8. Gt nanocrystals appear as bright dots possibly to charge trapping. Due to this appearance they can be detected from Fh precursor. Top view A, D, E. Side view of rod-like Gt nanocrystals B, C. Micrographs collected at A) 1 h; B-E) □0.5 h. Scale Bar 100 nm.

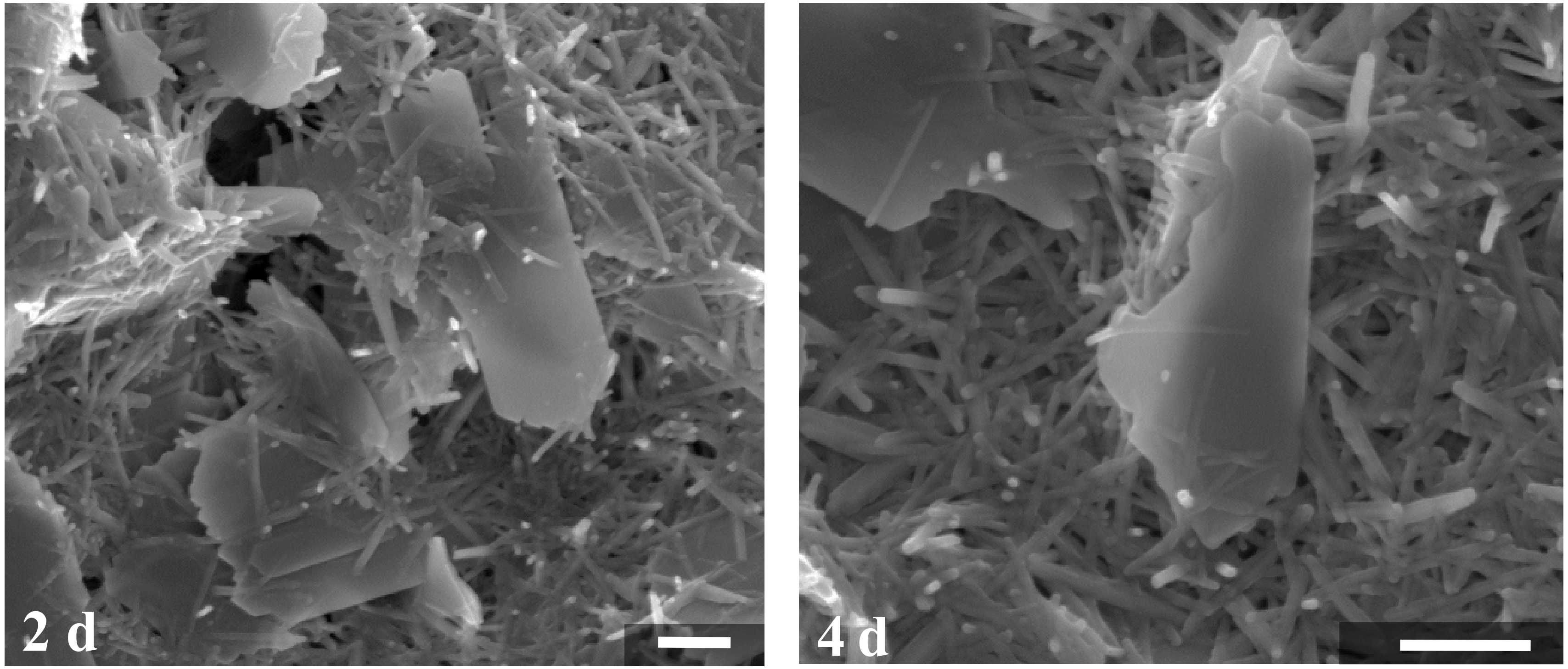

Fig. S9 SEM images from reaction of Fhy with 0.5 mM $FeCl_2$ and 10mM $_{HIGH}HCO^{-}_3$. No Fh was observed at 2 days reaction. Dissolution of Lp (right) at 4 d indicates its short residence time. Scale bar = 300 nm

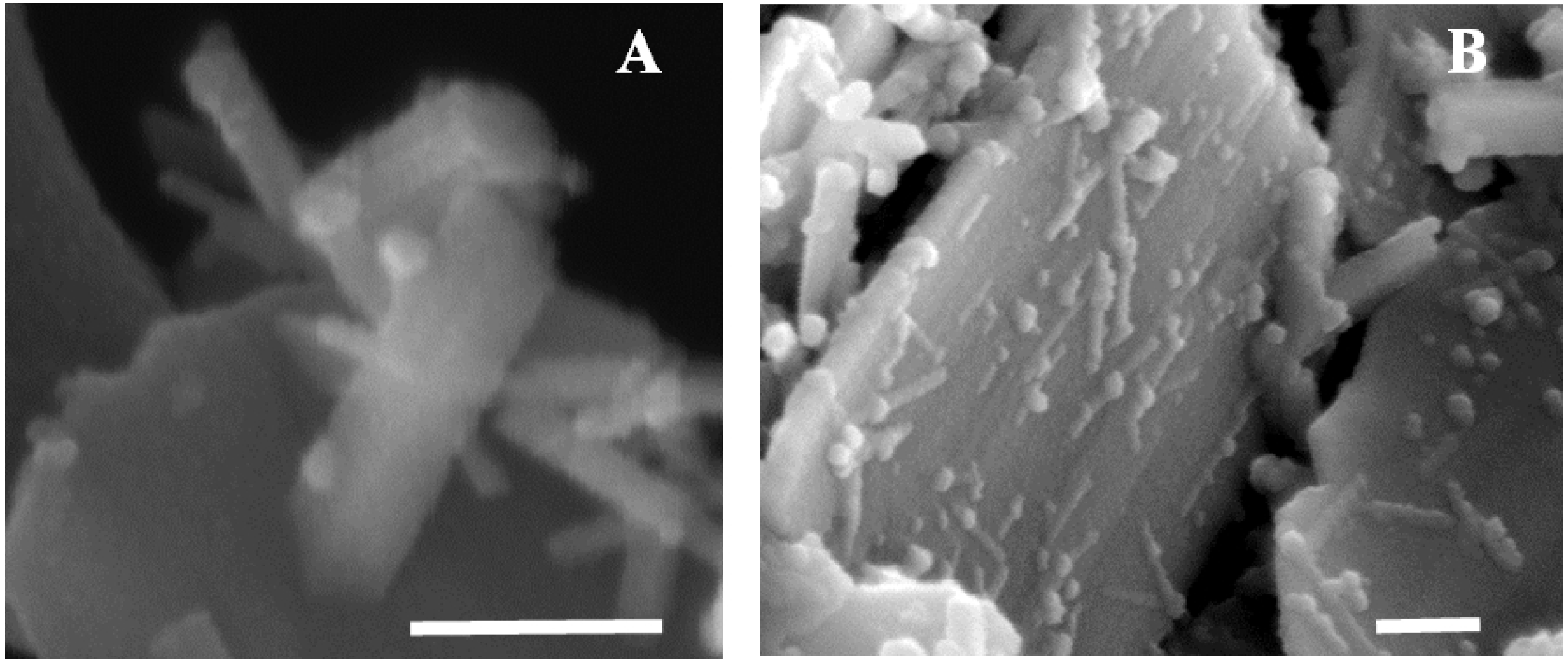

Fig. S10 SEM micrographs show: in A, elongated Gth particles forming rod-like crystals; in B, particles that appears aligned (oriented) in the direction of Gt rods. Images are from 5 days Fh reaction with 0.5 mM $FeCl_2$ ($_{NO}HCO^-_3$) and demonstrates that nucleation/growth of Gt is at the expense of Fh (note absence of Lp dissolution). Scale bar = 100 nm

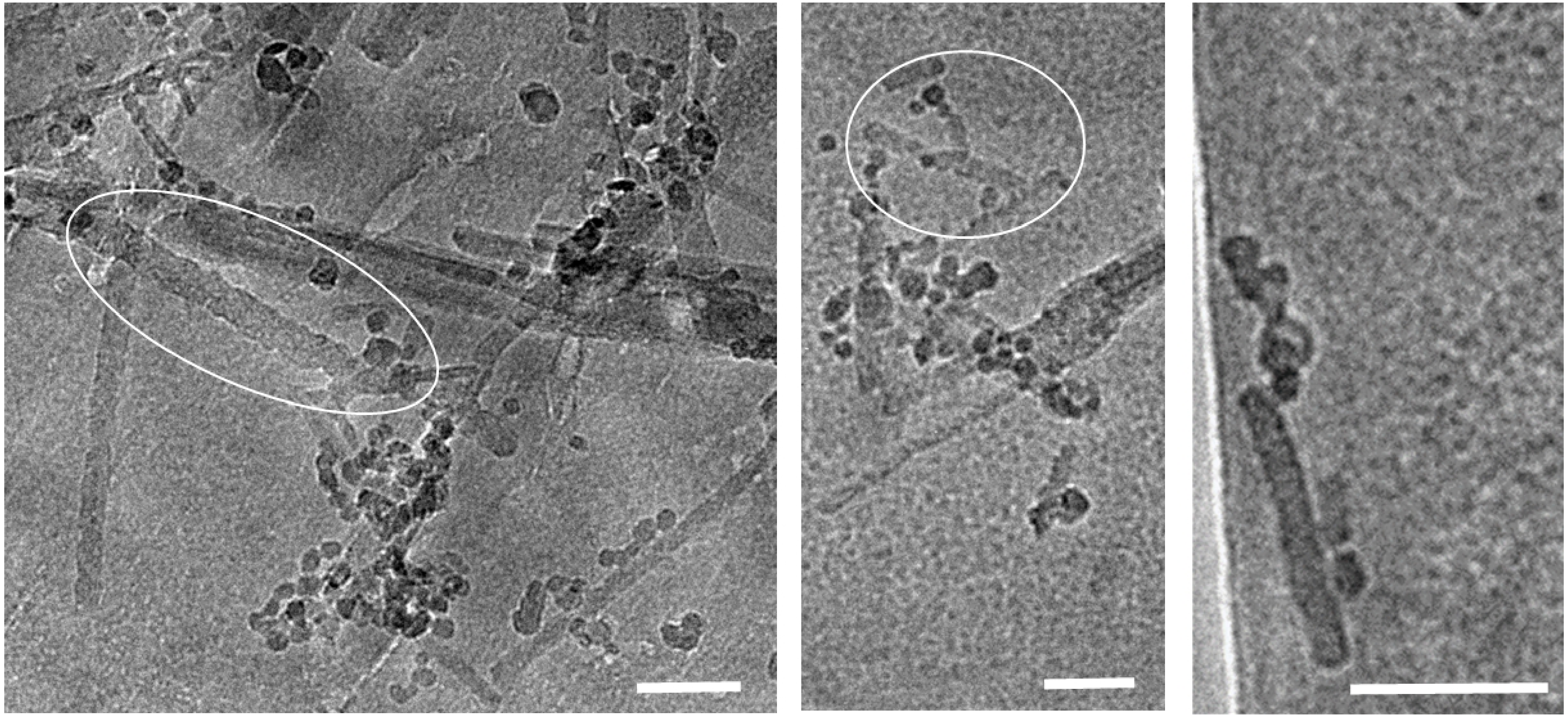

Fig. S11. TEM micrographs showing particles that appear aligned (oriented) in the direction of Gt rods. The data is from 5 days Fh reaction with 0.5mM $FeCl_2$ (0 HCO^-_3). Scale bar 20 nm.

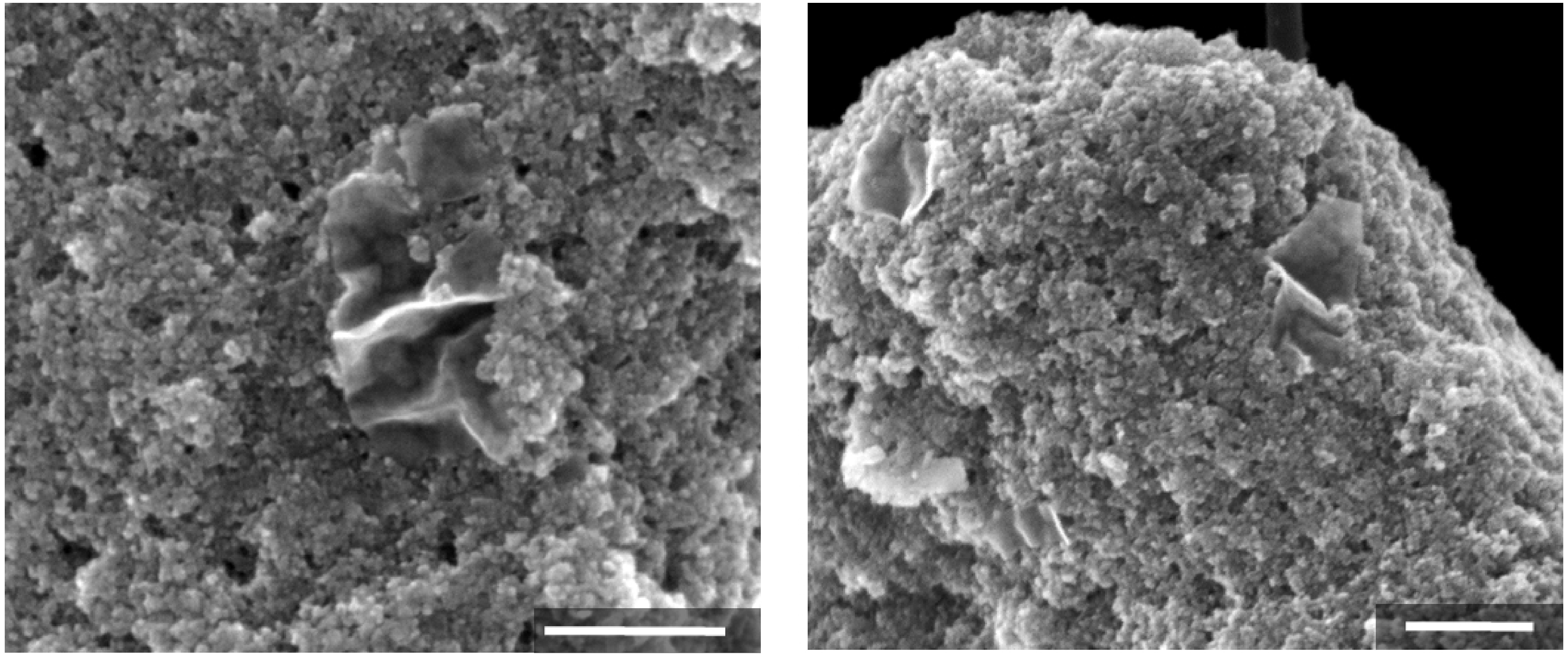

Fig. S12 Thin Lp crystals that formed after 0.75 h of Fh reaction with $FeCl_2$ appear to outline the Fh surface. Scale bar = 200nm

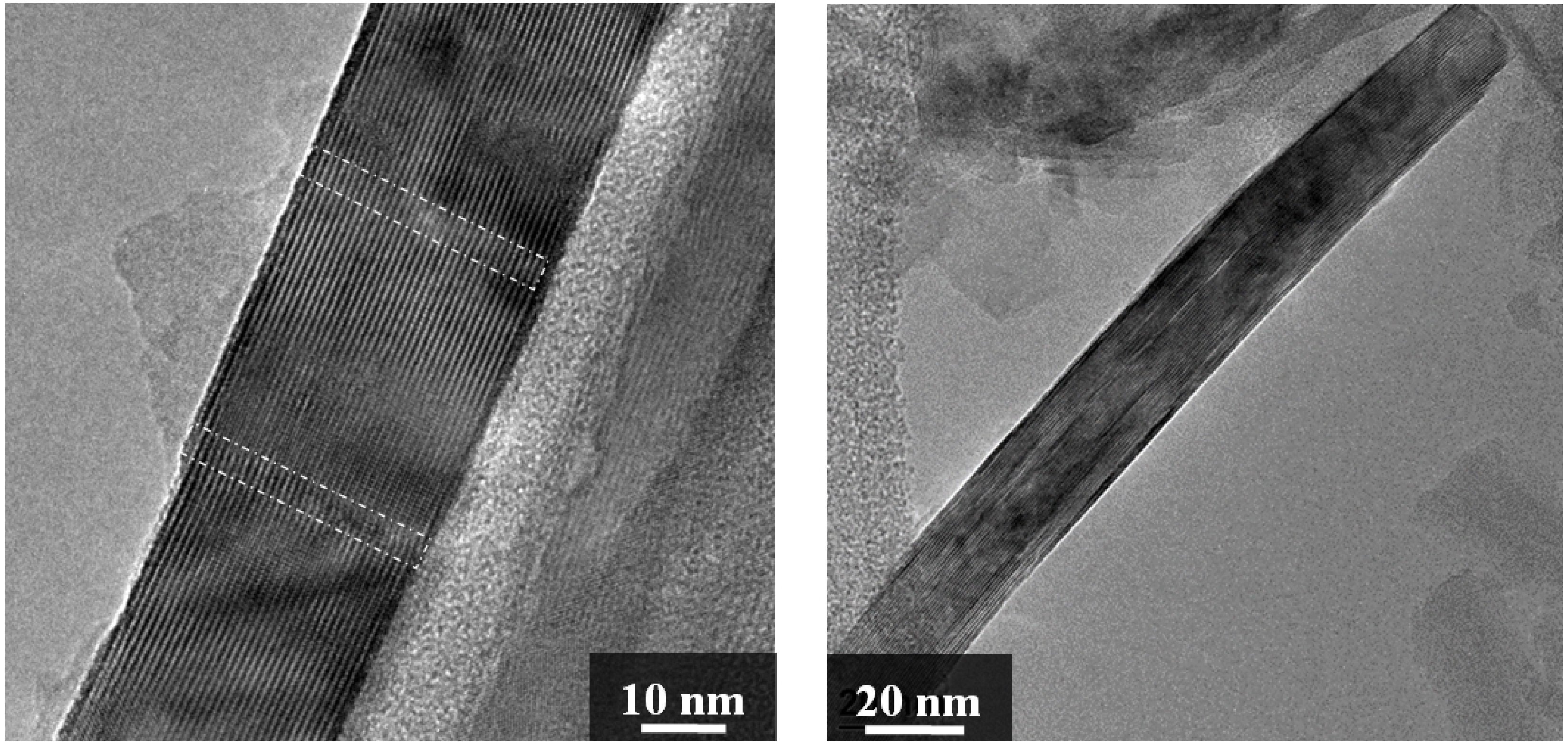

Fig. S13 TEM data shows staking faults on a Lp particle that are positioned at ~ 40 nm distance. Lp particles that grow by layer addition.

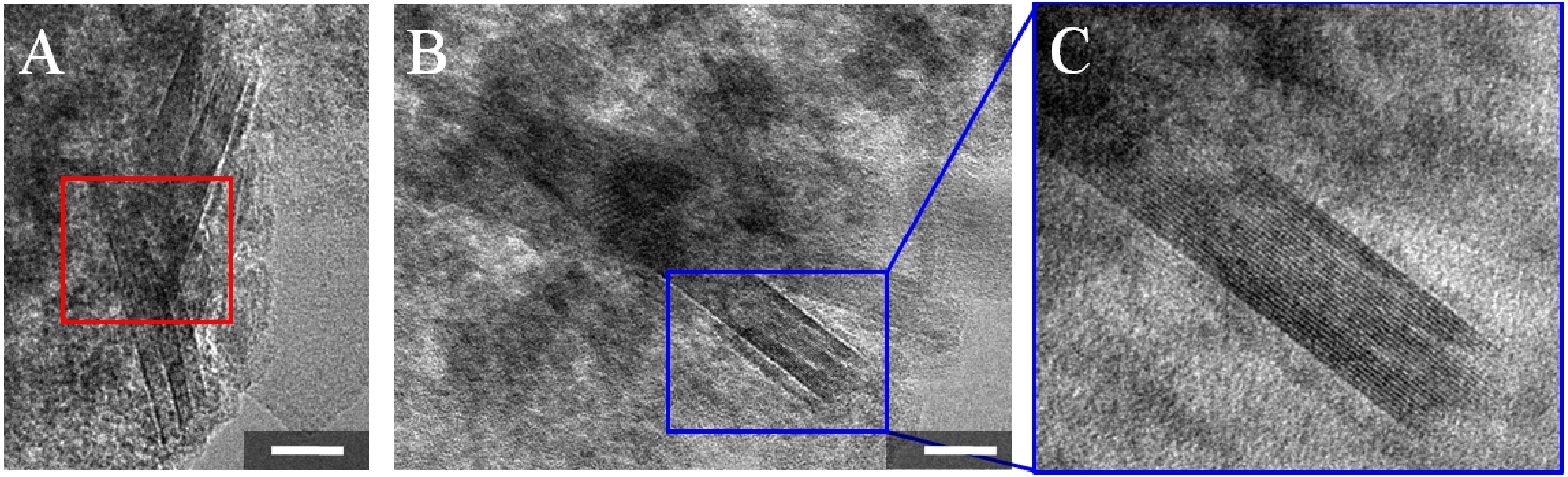

Fig. S14. TEM data at 2 h after reaction of Fh with $FeSO_4$. Micrographs depict Gt twinnig (red box in **A**); and particles that continue to grow in length with an irregular growth front (**B, C**). Identification of Gt based on d-spacing. Scale bar = 10 nm

Anion	Aqueous Fe(II) and (III) reactions			
	Fe(II)	logK	Fe(III)	logK
HCO_3^-	$Fe^{2+} + H^+ + CO_3^{2-} = FeHCO_3^+$	11.43	$Fe^{3+} + HCO_3^- = FeCO_3^+ + H^+$	-0.609
Cl^-	$Fe^{2+} + Cl^- = FeCl^+$	- 0.2	$Fe^{3+} + Cl^- = FeCl^{2+}$	1.48
SO_4^{2-}	$Fe^{2+} + SO_4^{2-} = FeSO_4$ (aq)	2.39	$Fe^{3+} + SO_4^{2-} = FeSO_4^+$	4.25
			$Fe^{3+} + 2SO_4^{2-} = Fe(SO_4)_2^-$	5.38

Table S3. Aqueous Fe(II) and Fe(III) complexes in solution, that pertain to experimental conditions

References

Christensen, A.N., Lehmann, M.S., Convert, P. (1982) *Acta Chemica Scandinavica, Series A*: **36** 303-308.

Ectors, D., Goetz-Neunhoeffer, F., and J. Neubauer, J., (2015) *J. Applied Crystallography*, **48**(1), 189-194.

Yang, H., Lu R., Downs R. T., Costin G. (2006) *Acta Crystallographica, Section E* **62** i250-i252.